Applied Mathematics Letters 173 (2026) 109770

Contents lists available at ScienceDirect

Applied Mathematics Letters

journal homepage: www.elsevier.com/locate/aml

Regular article

Inconsistent tensor-tensor product for low-rank tensor factorization

Sheng Liu, Xi-Le Zhao, Qin Jiang *

School of Mathematical Sciences, University of Electronic Science and Technology of China, China

ARTICLE INFO

Keywords:
Low-rank tensor completion
Inconsistent tensor-tensor product
Tensor factorization
Proximal alternating minimization

ABSTRACT

The tensor-tensor product (t-product) is a fundamental operation in tensor decomposition, enabling effective modeling of interactions between third-order tensors. However, the classical t-product is restricted by the fact that the two factors must have the same third-mode dimension, limiting its flexibility and expressiveness. To break this restriction, we introduce an inconsistent tensor-tensor product (it-product), which allows tensors with inconsistent third-mode dimensions to interact with each other while still respecting the algebraic structure of classical t-product. Equipped with the proposed it-product, we develop an it-product-based low-rank tensor factorization and suggest a unified model for tensor completion and tensor compression. To address the resulting nonconvex optimization problem, we build a proximal alternating minimization (PAM)-based algorithm. We further provide a theoretical convergence analysis, showing that the sequence generated by the algorithm converges to a critical point of the objective function under certain conditions. Numerical experiments on real-world datasets have been conducted to validate the effectiveness and superiority of the proposed method over existing baselines.

1. Introduction

In many data-rich fields, such as image processing [1] and video compression [2], most data can be modeled as tensors to characterize the inherent enrichment of information. Nevertheless, observed tensors in the real world often suffer from missing or corrupted conditions due to the limitations of devices and the environment, significantly hindering subsequent applications such as image classification, target detection, and data compression, to name but a few. Recovering underlying tensors from the partially observed tensors, i.e., tensor completion, is a classical inverse problem. Due to the inherent non-uniqueness and instability encountered in solving the inverse problem, it is an effective strategy to constrain the solution space by incorporating the prior information of tensors. Low-rankness, as a prior, has been widely utilized for extracting the internal structure of tensors in various real-world applications [3–5]. To characterize the low-rank prior of a tensor, tensor decompositions are investigated. The mainstream tensor decompositions include CANDECOMP/PARAFAC (CP) decomposition [6], Tucker decomposition [7,8], tensor network decomposition [9–11], and tensor singular value decomposition (T-SVD) [12–14].

The recent T-SVD and derived low-rank representations, induced by the tensor-tensor product (t-product), have attracted increasing attention due to their excellent ability in exploring low-rank structures of real-world data. Kilmer et al. [12] defined tensor tubal-rank and multi-rank with the framework of T-SVD by using circulant algebra, providing a new perspective on tensor decomposition. However, minimizing the multi-rank of a target tensor directly is an NP-hard problem, rendering its practical application computationally infeasible. To optimize this problem efficiently, Zhang et al. [15] introduced the tensor nuclear norm (TNN) as a convex relaxation of tensor multi-rank. Furthermore, Lu et al. [16] proposed the tensor average rank and designed a

* Corresponding author.
E-mail addresses: liusheng16@163.com (S. Liu), xlzhao122003@163.com (X.-L. Zhao), jiangqin0613@163.com (Q. Jiang).

https://doi.org/10.1016/j.aml.2025.109770
Received 19 August 2025; Received in revised form 19 September 2025; Accepted 19 September 2025
Available online 25 September 2025

corresponding TNN. Zhou et al. [17] proposed a tensor factorization method that decomposes a third-order tensor into the interaction of two smaller tensors based on the t-product, resulting in an efficient low-rank and SVD-free representation. Wu et al. [18] introduced a tensor QR-based low-rank representation and further defined a new form of TNN, extending the applicability of the classical TNN framework. Beyond these methods, Zhou et al. [19] introduced tensor low-rank representation (TLRR), which provides provable performance guarantees and can effectively recover clean data with low-rank structure. Although these low-rank tensor representations based on the t-product perform well in various applications, they usually rely on a fixed transform matrix, specifically the predefined discrete Fourier transform (DFT), which limits their flexibility for different data.

Recently, researchers have explored various transform matrices to overcome the limitations of predefined transforms in the T-SVD framework. Kernfeld et al. [13] declared that any invertible transform can serve as a transform matrix for the generalized t-product. Lu et al. [20] utilized the discrete cosine transform (DCT) to replace the DFT and proved the exact recovery guarantees of the proposed model. Song et al. [21] further extended this idea by advocating the use of general unitary matrices instead of the DFT. To better explore the low-rank structure of tensors, increasing attention has been paid to using non-invertible matrices as transform matrices in defining the TNN. For example, Jiang et al. [22] first proposed a semi-invertible framelet transform in defining the TNN, thus breaking away from the strict requirement of full invertibility. Subsequently, many researchers have considered different non-invertible transforms to serve as the transform matrix, such as learnable non-invertible transform [23,24], nonlinear transform [25], and deep neural network [26,27], to name but a few. Despite the great success of the above-mentioned transform-based low-rank representations, they still require the use of the same transform matrix for different interacting tensor factors, due to the dimensional consistency constraint, which hinders their flexibility and extensibility.

To break the dimensional consistency constraint inherent in the classical t-product, we introduce an inconsistent tensor-tensor product (it-product) defined along the third-mode dimension, which allows the two interaction factors to be inconsistent in the third-mode dimension, thereby enhancing the flexibility of the classical t-product. Specifically, the it-product aligns tensors with inconsistent third-mode dimensions by mapping them into a dimension-consistent transform domain through different transform matrices, where their interactions are performed, and then remaps the operation result to the original domain. The main contributions of this paper are twofold:

(1) We introduce an it-product, which allows the interaction between tensors with inconsistent third-mode dimensions while still respecting the algebraic structure of classical t-product. Building upon this, we develop an it-product-based low-rank tensor factorization and suggest a unified model for tensor completion and tensor compression to verify its effectiveness.

(2) We develop a proximal alternating minimization (PAM)-based algorithm for the resulting optimization problem. We further provide a theoretical convergence analysis, showing that the sequence generated by the algorithm converges to a critical point of the objective function. Extensive experiments on real-world datasets have confirmed the superior performance of the proposed method compared to existing baselines.

2. Notations and preliminaries

The following notations and definitions are used throughout this paper. Scalars, vectors, matrices, and tensors are represented by x, $\boldsymbol{x}$, $\boldsymbol{X}$, and $\mathcal{X}$, respectively. For a matrix $\boldsymbol{X} \in \mathbb{R}^{n_1 \times n_2}$, its transpose is denoted by $\boldsymbol{X}^\top$. The Frobenius norm of a tensor $\mathcal{X}$ is denoted as $\|\mathcal{X}\|_F$. The mode-p matricization (or unfolding) of a tensor $\mathcal{X}$ is denoted as $\boldsymbol{X}_{(p)} = \mathrm{unfold}_p(\mathcal{X})$, which maps $\mathcal{X}$ into a matrix in $\mathbb{R}^{n_p \times (n_1 \cdots n_{p-1} n_{p+1} \cdots n_N)}$. Its inverse operation, folding the matrix back into the original tensor structure, is denoted as $\mathcal{X} = \mathrm{fold}_p(\boldsymbol{X}_{(p)})$. The kth frontal slice of $\mathcal{X}$ is denoted as $\boldsymbol{X}^{(k)} = \mathcal{X}(:,:,k)$.

Definition 1 (*Tensor-Tensor Product [12,13]*)**.** For third-order tensors $\mathcal{G} \in \mathbb{R}^{n_1 \times n_2 \times n_3}$, $\mathcal{A} \in \mathbb{R}^{n_1 \times r \times n_3}$, and $\mathcal{B} \in \mathbb{R}^{r \times n_2 \times n_3}$, the tensor-tensor product (t-product) is defined as

$$\mathcal{G} = \mathcal{A} * \mathcal{B} = \left(\left(\mathcal{A} \times_3 \boldsymbol{F} \right) \triangle_3 \left(\mathcal{B} \times_3 \boldsymbol{F} \right) \right) \times_3 \boldsymbol{F}^{-1}, \tag{1}$$

where $\boldsymbol{F} \in \mathbb{C}^{n_3 \times n_3}$ is DFT matrix, $\times_3$ is mode-3 tensor-matrix product [8], and $\triangle_3$ is face-wise product [13].

As shown in Eq. (1), the cornerstone of the classical t-product is the transform matrix, which converts the convolution operation in the original domain into a face-wise product in the transform domain. From Eq. (1), two interaction factors ($\mathcal{A} \in \mathbb{R}^{n_1 \times r \times n_3}$ and $\mathcal{B} \in \mathbb{R}^{r \times n_2 \times n_3}$) share the same dimensional transform matrix (DFT matrix $\boldsymbol{F} \in \mathbb{C}^{n_3 \times n_3}$), this restriction comes from the fact that the third dimensions of $\mathcal{A}$ and $\mathcal{B}$ must be the same. This dimensional consistency constraint limits the applicability of the classical t-product to tensors with the same size in the third dimension. To overcome this restriction, we introduce a flexible extension of the classical t-product, defined as follows.

Definition 2 (*Inconsistent Tensor-Tensor Product*)**.** Let $\mathcal{A} \in \mathbb{R}^{n_1 \times r \times \ell_1}$ and $\mathcal{B} \in \mathbb{R}^{r \times n_2 \times \ell_2}$ be two third-order tensors, where the tube lengths ℓ_1 and ℓ_2 are not necessarily equal, i.e., $\ell_1 \neq \ell_2$ is allowed. The inconsistent tensor-tensor product (it-product) between $\mathcal{A}$ and $\mathcal{B}$ results in third order tensor $\mathcal{G} \in \mathbb{R}^{n_1 \times n_2 \times n_3}$, defined as

$$\mathcal{G} = \mathcal{A} \square \mathcal{B} = \left(\left(\mathcal{A} \times_3 \boldsymbol{T}_1 \right) \triangle_3 \left(\mathcal{B} \times_3 \boldsymbol{T}_2 \right) \right) \times_3 \boldsymbol{T}_3, \tag{2}$$

where $\boldsymbol{T}_1 \in \mathbb{R}^{\ell_3 \times \ell_1}$, $\boldsymbol{T}_2 \in \mathbb{R}^{\ell_3 \times \ell_2}$, $\boldsymbol{T}_3 \in \mathbb{R}^{n_3 \times \ell_3}$ are alignment transform matrices, and $\triangle_3$ is face-wise product [13].

As shown in Eq. (2), the two interaction tensor factors ($\mathcal{A} \in \mathbb{R}^{n_1 \times r \times \ell_1}$ and $\mathcal{B} \in \mathbb{R}^{r \times n_2 \times \ell_2}$) are not necessarily equal in the third dimension (i.e., $\ell_1 \neq \ell_2$ is allowed), and they can be mapped to a transform domain with the same dimension by different alignment transform matrices. Moreover, when the alignment transforms $\boldsymbol{T}_1$ and $\boldsymbol{T}_2$ are chosen as the DFT matrices and $\boldsymbol{T}_3$ is the corresponding inverse DFT, the proposed it-product reduces to the classical t-product as a special case. The proposed framework thus extends the classical t-product to handle tensors with inconsistent third-mode dimensions, while still respecting its essential algebraic structure.

3. The proposed model

Inspired by the proposed it-product (Definition 2), we develop a novel low-rank tensor factorization for tensor completion and data compression tasks, which can be formulated as follows:

$$\min_{\mathcal{X},\mathcal{A},\mathcal{B},\boldsymbol{T}_i} \frac{1}{2}\|\mathcal{X}-\left(\left(\mathcal{A}\times_3 \boldsymbol{T}_1\right)\triangle_3\left(\mathcal{B}\times_3 \boldsymbol{T}_2\right)\right)\times_3 \boldsymbol{T}_3\|_F^2+\frac{\gamma}{2}\left(\|\mathcal{A}\|_F^2+\|\mathcal{B}\|_F^2\right)\ \text{s.t. } \mathcal{P}_{\Omega}(\mathcal{X})=\mathcal{P}_{\Omega}(\mathcal{O}),\|\boldsymbol{T}_i(:,k)\|_F^2=1. \tag{3}$$

Here, $\mathcal{O}$ denotes the observed tensor, $\mathcal{X}$ is the recovered tensor, and $i=1,2,3$. The operator $\mathcal{P}_{\Omega}(\cdot)$ denotes the projection that retains the entries indexed by Ω while setting all others to zero. For data compression, Ω corresponds to the full observation index, and the compressed representation consists of the factors $\mathcal{A}$, $\mathcal{B}$, and $\boldsymbol{T}_i$. By introducing auxiliary variables together with the indicator functions $\Phi(\mathcal{X})$ and $\Psi(\boldsymbol{T}_i)$ defined as follows, To tackle this optimization problem, we introduce the auxiliary variables $\mathcal{Z}=\mathcal{M}\triangle_3\mathcal{N}$, $\mathcal{M}=\mathcal{A}\times_3\boldsymbol{T}_1$, $\mathcal{N}=\mathcal{B}\times_3\boldsymbol{T}_2$, and the indicator functions $\Phi(\mathcal{X})$ and $\Psi(\boldsymbol{T}_i)$ defined as follows,

$$\Phi(\mathcal{X})=\begin{cases}0, & \mathcal{P}_{\Omega}(\mathcal{X})=\mathcal{P}_{\Omega}(\mathcal{O}),\\ +\infty, & otherwise,\end{cases}\quad\text{and}\quad \Psi\left(\boldsymbol{T}_i\right)=\begin{cases}0, & \|\boldsymbol{T}_i(:,k)\|_F^2=1,\\ +\infty, & otherwise,\end{cases} \tag{4}$$

the problem (3) can be reformulated as:

$$\begin{aligned}\min_{\mathcal{X},\mathcal{Z},\mathcal{M},\mathcal{N},\mathcal{A},\mathcal{B},\boldsymbol{T}_i}\ &\frac{1}{2}\|\mathcal{X}-\mathcal{Z}\times_3\boldsymbol{T}_3\|_F^2+\frac{\mu}{2}\|\mathcal{Z}-\mathcal{M}\triangle_3\mathcal{N}\|_F^2+\Phi(\mathcal{X})+\Psi\left(\boldsymbol{T}_1\right)+\Psi\left(\boldsymbol{T}_2\right)+\Psi\left(\boldsymbol{T}_3\right)\\ &+\frac{\alpha}{2}\|\mathcal{M}-\mathcal{A}\times_3\boldsymbol{T}_1\|_F^2+\frac{\beta}{2}\|\mathcal{N}-\mathcal{B}\times_3\boldsymbol{T}_2\|_F^2+\frac{\gamma}{2}\left(\|\mathcal{A}\|_F^2+\|\mathcal{B}\|_F^2\right).\end{aligned} \tag{5}$$

3.1. Solving algorithm for the proposed model

Within the proximal alternating minimization (PAM) framework, the variables $\mathcal{X},\mathcal{Z},\mathcal{M},\mathcal{N},\mathcal{A},\mathcal{B}$, and $\boldsymbol{T}_i$ in Eq. (5) are updated in an alternating manner as follows:

$$\begin{cases}\mathcal{X}^{t+1}=\arg\min_{\mathcal{X}}\mathcal{L}\left(\mathcal{X},\mathcal{Z}^t,\mathcal{M}^t,\mathcal{N}^t,\mathcal{A}^t,\mathcal{B}^t,\boldsymbol{T}_i^t\right)+\frac{\rho}{2}\|\mathcal{X}-\mathcal{X}^t\|_F^2,\\ \mathcal{Z}^{t+1}=\arg\min_{\mathcal{Z}}\mathcal{L}\left(\mathcal{X}^{t+1},\mathcal{Z},\mathcal{M}^t,\mathcal{N}^t,\mathcal{A}^t,\mathcal{B}^t,\boldsymbol{T}_i^t\right)+\frac{\rho}{2}\|\mathcal{Z}-\mathcal{Z}^t\|_F^2,\\ \mathcal{M}^{t+1}=\arg\min_{\mathcal{M}}\mathcal{L}\left(\mathcal{X}^{t+1},\mathcal{Z}^{t+1},\mathcal{M},\mathcal{N}^t,\mathcal{A}^t,\mathcal{B}^t,\boldsymbol{T}_i^t\right)+\frac{\rho}{2}\|\mathcal{M}-\mathcal{M}^t\|_F^2,\\ \mathcal{N}^{t+1}=\arg\min_{\mathcal{N}}\mathcal{L}\left(\mathcal{X}^{t+1},\mathcal{Z}^{t+1},\mathcal{M}^{t+1},\mathcal{N},\mathcal{A}^t,\mathcal{B}^t,\boldsymbol{T}_i^t\right)+\frac{\rho}{2}\|\mathcal{N}-\mathcal{N}^t\|_F^2,\\ \mathcal{A}^{t+1}=\arg\min_{\mathcal{A}}\mathcal{L}\left(\mathcal{X}^{t+1},\mathcal{Z}^{t+1},\mathcal{M}^{t+1},\mathcal{N}^{t+1},\mathcal{A},\mathcal{B}^t,\boldsymbol{T}_i^t\right)+\frac{\rho}{2}\|\mathcal{A}-\mathcal{A}^t\|_F^2,\\ \mathcal{B}^{t+1}=\arg\min_{\mathcal{B}}\mathcal{L}\left(\mathcal{X}^{t+1},\mathcal{Z}^{t+1},\mathcal{M}^{t+1},\mathcal{N}^{t+1},\mathcal{A}^{t+1},\mathcal{B},\boldsymbol{T}_i^t\right)+\frac{\rho}{2}\|\mathcal{B}-\mathcal{B}^t\|_F^2,\\ \boldsymbol{T}_i^{t+1}=\arg\min_{\boldsymbol{T}_i}\mathcal{L}\left(\mathcal{X}^{t+1},\mathcal{Z}^{t+1},\mathcal{M}^{t+1},\mathcal{N}^{t+1},\mathcal{A}^{t+1},\mathcal{B}^{t+1},\boldsymbol{T}_i\right)+\frac{\rho}{2}\|\boldsymbol{T}_i-\boldsymbol{T}_i^t\|_F^2.\end{cases} \tag{6}$$

where $\mathcal{L}\left(\mathcal{X},\mathcal{Z},\mathcal{M},\mathcal{N},\mathcal{A},\mathcal{B},\boldsymbol{T}_i\right)$ is the objective function in Eq. (5) and $\rho>0$ is the proximal parameter.

(1) Solving the $\mathcal{X}$-subproblem: $\mathcal{X}^{t+1}\in\arg\min_{\mathcal{X}}\frac{1}{2}\|\mathcal{X}-\mathcal{Z}^t\times_3\boldsymbol{T}_3^t\|_F^2+\frac{\rho}{2}\|\mathcal{X}-\mathcal{X}^t\|_F^2+\Phi(\mathcal{X})$. The closed-form solution is given by

$$\mathcal{X}^{t+1}=\mathcal{P}_{\Omega^C}\left(\frac{\mathcal{Z}^t\times_3\boldsymbol{T}_3^t+\rho\mathcal{X}^t}{1+\rho}\right)+\mathcal{P}_{\Omega}(\mathcal{O}). \tag{7}$$

(2) Solving the $\mathcal{Z}$-subproblem: $\mathcal{Z}^{t+1}\in\arg\min_{\mathcal{Z}}\frac{1}{2}\|\mathcal{X}^{t+1}-\mathcal{Z}\times_3\boldsymbol{T}_3^t\|_F^2+\frac{\mu}{2}\|\mathcal{Z}-\mathcal{M}^t\triangle_3\mathcal{N}^t\|_F^2+\frac{\rho}{2}\|\mathcal{Z}-\mathcal{Z}^t\|_F^2$. The closed-form solution is given by

$$\mathcal{Z}^{t+1}=\text{Fold}\left(\left(\left(\boldsymbol{T}_3^t\right)^{\top}\boldsymbol{T}_3^t+(\mu+\rho)\boldsymbol{I}\right)^{-1}\left(\left(\boldsymbol{T}_3^t\right)^{\top}\boldsymbol{X}_{(3)}^{t+1}+\mu\boldsymbol{H}_{(3)}^t+\rho\boldsymbol{Z}_{(3)}^t\right)\right), \tag{8}$$

where $\boldsymbol{H}_{(3)}^t$ is the mode-3 matricization of $\mathcal{H}^t$ and $\mathcal{H}^t=\mathcal{M}^t\triangle_3\mathcal{N}^t$.

(3) Solving the $\mathcal{M}$-subproblem: $\mathcal{M}^{t+1}\in\arg\min_{\mathcal{M}}\frac{\mu}{2}\|\mathcal{Z}^{t+1}-\mathcal{M}\triangle_3\mathcal{N}^t\|_F^2+\frac{\alpha}{2}\|\mathcal{M}-\mathcal{A}^t\times_3\boldsymbol{T}_1^t\|_F^2+\frac{\rho}{2}\|\mathcal{M}-\mathcal{M}^t\|_F^2$. This subproblem decouples into ℓ_3 independent problems along the third-mode dimension. The closed-form solution for the kth slice is:

$$\boldsymbol{M}^{(k)}=\left(\mu\boldsymbol{Z}^{(k)}\left(\boldsymbol{N}^{(k)}\right)^{\top}+\alpha\boldsymbol{P}^{(k)}+\rho\hat{\boldsymbol{M}}^{(k)}\right)\left(\mu\boldsymbol{N}^{(k)}\left(\boldsymbol{N}^{(k)}\right)^{\top}+(\alpha+\rho)\boldsymbol{I}\right)^{-1}, \tag{9}$$

where $\boldsymbol{M}^{(k)},\boldsymbol{N}^{(k)},\boldsymbol{Z}^{(k)},\boldsymbol{P}^{(k)}$, and $\hat{\boldsymbol{M}}^{(k)}$ denote the kth slices of $\mathcal{M},\mathcal{N}^t,\mathcal{Z}^{t+1},\mathcal{P}^t$, and $\mathcal{M}^t$, with $\mathcal{P}^t=\mathcal{A}^t\times_3\boldsymbol{T}_1^t$.

(4) Solving the $\mathcal{N}$-subproblem: $\mathcal{N}^{t+1}\in\arg\min_{\mathcal{N}}\frac{\mu}{2}\|\mathcal{Z}^{t+1}-\mathcal{M}^{t+1}\triangle_3\mathcal{N}\|_F^2+\frac{\beta}{2}\|\mathcal{N}-\mathcal{B}^t\times_3\boldsymbol{T}_2^t\|_F^2+\frac{\rho}{2}\|\mathcal{N}-\mathcal{N}^t\|_F^2$. This subproblem decouples into ℓ_3 independent problems along the third-mode dimension. The closed-form solution for the kth slice is:

$$\boldsymbol{N}^{(k)}=\left(\mu\left(\boldsymbol{M}^{(k)}\right)^{\top}\boldsymbol{M}^{(k)}+(\beta+\rho)\boldsymbol{I}\right)^{-1}\left(\mu\left(\boldsymbol{M}^{(k)}\right)^{\top}\boldsymbol{Z}^{(k)}+\alpha\boldsymbol{Q}^{(k)}+\rho\hat{\boldsymbol{N}}^{(k)}\right), \tag{10}$$

where $\boldsymbol{N}^{(k)},\boldsymbol{M}^{(k)},\boldsymbol{Z}^{(k)},\boldsymbol{Q}^{(k)}$, and $\hat{\boldsymbol{N}}^{(k)}$ denote the kth slices of $\mathcal{N},\mathcal{M}^{t+1},\mathcal{Z}^{t+1},\mathcal{Q}^t$, and $\mathcal{N}^t$, with $\mathcal{Q}^t=\mathcal{B}^t\times_3\boldsymbol{T}_2^t$.

Algorithm 1 PAM algorithm for the proposed model.

Input: The observed tensor $\mathcal{O} \in \mathbb{R}^{n_1 \times n_2 \times n_3}$, the index Ω, the parameter $r, \ell_1, \ell_2, \ell_3$, α, β, γ, μ, ρ, and the maximum iteration $t_{max} = 1000$.

Output: The recovered tensor $\mathcal{X} \in \mathbb{R}^{n_1 \times n_2 \times n_3}$.

1: **Initialization:** The iteration $t = 0$, $\mathcal{X}^0, \mathcal{Z}^0, \mathcal{M}^0, \mathcal{N}^0, \mathcal{A}^0, \mathcal{B}^0$, and $\boldsymbol{T}_i^0$.
2: **while** not converged and $t < t_{max}$ **do**
3: Update $\mathcal{X}^{t+1}$ via Eq. (7); Update $\mathcal{Z}^{t+1}$ via Eq. (8); Update $\mathcal{M}^{t+1}$ via Eq. (9); Update $\mathcal{N}^{t+1}$ via Eq. (10);
4: Update $\mathcal{A}^{t+1}$ via Eq. (11); Update $\mathcal{B}^{t+1}$ via Eq. (12); Update $\boldsymbol{T}_i^{t+1}$ via Eq. (13) for $i = 1, 2, 3$; Let $t = t + 1$;
5: Check the convergence condition: $\left\|\mathcal{X}^{t+1} - \mathcal{X}^t\right\|_F / \left\|\mathcal{X}^t\right\|_F \leq 10^{-5}$;
6: **end while**

(5) Solving the $\mathcal{A}$-subproblem: $\mathcal{A}^{t+1} \in \arg\min_{\mathcal{A}} \frac{\alpha}{2}\|\mathcal{M}^{t+1} - \mathcal{A} \times_3 \boldsymbol{T}_1^t\|_F^2 + \frac{\gamma}{2}\|\mathcal{A}\|_F^2 + \frac{\rho}{2}\|\mathcal{A} - \mathcal{A}^t\|_F^2$. The closed-form solution to this subproblem is

$$\mathcal{A}^{t+1} = \text{Fold}_3\left(\left(\alpha\left(\boldsymbol{T}_1^t\right)^\top \boldsymbol{T}_1^t + (\gamma + \rho)\boldsymbol{I}\right)^{-1}\left(\left(\boldsymbol{T}_1^t\right)^\top \boldsymbol{M}_{(3)}^{t+1} + \rho \boldsymbol{A}_{(3)}^t\right)\right). \tag{11}$$

(6) Solving the $\mathcal{B}$-subproblem: $\mathcal{B}^{t+1} \in \arg\min_{\mathcal{B}} \frac{\beta}{2}\|\mathcal{N}^{t+1} - \mathcal{B} \times_3 \boldsymbol{T}_2^t\|_F^2 + \frac{\gamma}{2}\|\mathcal{B}\|_F^2 + \frac{\rho}{2}\|\mathcal{B} - \mathcal{B}^t\|_F^2$. The closed-form solution to this subproblem is

$$\mathcal{B}^{t+1} = \text{Fold}_3\left(\left(\beta\left(\boldsymbol{T}_2^t\right)^\top \boldsymbol{T}_2^t + (\gamma + \rho)\boldsymbol{I}\right)^{-1}\left(\left(\boldsymbol{T}_2^t\right)^\top \boldsymbol{N}_{(3)}^{t+1} + \rho \boldsymbol{B}_{(3)}^t\right)\right). \tag{12}$$

(7) Solving the $\boldsymbol{T}_1$-subproblem: $\boldsymbol{T}_1^{t+1} \in \arg\min_{\boldsymbol{T}_1} \frac{\alpha}{2}\|\mathcal{M}^{t+1} - \mathcal{A}^{t+1} \times_3 \boldsymbol{T}_1\|_F^2 + \frac{\rho}{2}\|\boldsymbol{T}_1 - \boldsymbol{T}_1^t\|_F^2 + \Psi\left(\boldsymbol{T}_1\right)$. Following the strategy in [28], $\boldsymbol{T}_1^{t+1}$ is updated column by column. For each column vector $\boldsymbol{t}_1^k$, the solution is given by:

$$(\boldsymbol{t}_1^k)^{t+1} = \alpha \boldsymbol{W}^t \boldsymbol{a}_k^{t+1} + \rho(\boldsymbol{t}_1^k)^t / \|\alpha \boldsymbol{w}^t \boldsymbol{a}_k^{t+1} + \rho(\boldsymbol{t}_1^k)^t\|_F^2, \tag{13}$$

where $\boldsymbol{W}^t = \boldsymbol{M}_{(3)}^{t+1} - \sum_{i \neq k} (\boldsymbol{t}^i)^t (\boldsymbol{a}_i)^{t+1}$ and $\boldsymbol{A}_{(3)}^{t+1} = [(\boldsymbol{a}_1)^{t+1}, \ldots, (\boldsymbol{a}_{\ell_1})^{t+1}]^\top$. The updates for $\boldsymbol{T}_2$ and $\boldsymbol{T}_3$ follow the same procedure and are omitted for brevity.

3.2. Computational complexity analysis

For a third-order tensor $\mathcal{X} \in \mathbb{R}^{n_1 \times n_2 \times n_3}$ with rank parameter r and transform matrix parameters ℓ_1, ℓ_2, ℓ_3, the main computational cost per iteration arises from updating $\mathcal{X}$, $\mathcal{Z}$, $\mathcal{M}$, $\mathcal{N}$, $\mathcal{A}$, $\mathcal{B}$, $\boldsymbol{T}_1$, $\boldsymbol{T}_2$, and $\boldsymbol{T}_3$, which are $\mathcal{O}(n_1 n_2 n_3 \ell_3)$, $\mathcal{O}(n_1 n_2 n_3 \ell_3)$, $\mathcal{O}(n_1 n_2 r \ell_3)$, $\mathcal{O}(n_1 n_2 r \ell_3)$, $\mathcal{O}(n_1 n_2 \ell_1 \ell_3)$, $\mathcal{O}(n_1 n_2 \ell_2 \ell_3)$, $\mathcal{O}(n_1 n_2 \ell_1^2)$, $\mathcal{O}(n_1 n_2 \ell_2^2)$, and $\mathcal{O}(n_1 n_2 \ell_3^2)$, respectively. Therefore, the overall computational complexity per iteration of Algorithm 1 is $\mathcal{O}(n_1 n_2((n_3 + r + \ell_1 + \ell_2)\ell_3 + \ell_1^2 + \ell_2^2 + \ell_3^2))$.

3.3. Convergence analysis

This section presents the theoretical convergence analysis of our algorithm. For clarity, we denote the objective function of problem as $\mathcal{L}\left(\mathcal{X}, \mathcal{Z}, \mathcal{M}, \mathcal{N}, \mathcal{A}, \mathcal{B}, \boldsymbol{T}_i\right)$, $\mathcal{V} \triangleq \left\{\mathcal{X}, \mathcal{Z}, \mathcal{M}, \mathcal{N}, \mathcal{A}, \mathcal{B}, \boldsymbol{T}_i\right\}$, and

$$\mathcal{G}(\mathcal{V}) = \frac{1}{2}\|\mathcal{X} - \mathcal{Z} \times_3 \boldsymbol{T}_3\|_F^2 + \frac{\mu}{2}\|\mathcal{Z} - \mathcal{M} \triangle \mathcal{N}\|_F^2 + \frac{\alpha}{2}\|\mathcal{M} - \mathcal{A} \times_3 \boldsymbol{T}_1\|_F^2 + \frac{\beta}{2}\|\mathcal{N} - \mathcal{B} \times_3 \boldsymbol{T}_2\|_F^2 + \frac{\gamma}{2}\left(\|\mathcal{A}\|_F^2 + \|\mathcal{B}\|_F^2\right).$$

Theorem 1. *Assume that the sequence $\left\{\mathcal{X}^t, \mathcal{Z}^t, \mathcal{M}^t, \mathcal{N}^t, \mathcal{A}^t, \mathcal{B}^t, \boldsymbol{T}_i^t\right\}_{t \in \mathbb{N}}$ is generated by the Algorithm 1 and satisfies the following properties*

1. *The sequence $\left\{\mathcal{X}^t, \mathcal{Z}^t, \mathcal{M}^t, \mathcal{N}^t, \mathcal{A}^t, \mathcal{B}^t, \boldsymbol{T}_i^t\right\}_{t \in \mathbb{N}}$ satisfies the sufficient decrease condition.*
2. *The sequence $\left\{\mathcal{X}^t, \mathcal{Z}^t, \mathcal{M}^t, \mathcal{N}^t, \mathcal{A}^t, \mathcal{B}^t, \boldsymbol{T}_i^t\right\}_{t \in \mathbb{N}}$ is bounded.*
3. *The sequence $\left\{\mathcal{X}^t, \mathcal{Z}^t, \mathcal{M}^t, \mathcal{N}^t, \mathcal{A}^t, \mathcal{B}^t, \boldsymbol{T}_i^t\right\}_{t \in \mathbb{N}}$ satisfies the relative error condition.*
4. *$\mathcal{L}\left(\mathcal{X}^t, \mathcal{Z}^t, \mathcal{M}^t, \mathcal{N}^t, \mathcal{A}^t, \mathcal{B}^t, \boldsymbol{T}_i^t\right)$ has the Kurdyka-Łojasiewicz property at $\left(\mathcal{X}^t, \mathcal{Z}^t, \mathcal{M}^t, \mathcal{N}^t, \mathcal{A}^t, \mathcal{B}^t, \boldsymbol{T}_i^t\right)_{t \in \mathbb{N}}$.*
5. *$\mathcal{L}\left(\mathcal{X}^t, \mathcal{Z}^t, \mathcal{M}^t, \mathcal{N}^t, \mathcal{A}^t, \mathcal{B}^t, \boldsymbol{T}_i^t\right)$ satisfies the continuity condition.*

Then, the sequence $\left\{\mathcal{X}^t, \mathcal{Z}^t, \mathcal{M}^t, \mathcal{N}^t, \mathcal{A}^t, \mathcal{B}^t, \boldsymbol{T}_i^t\right\}_{t \in \mathbb{N}}$ converges to a stationary point $\left(\mathcal{X}^*, \mathcal{Z}^*, \mathcal{M}^*, \mathcal{N}^*, \mathcal{A}^*, \mathcal{B}^*, \boldsymbol{T}_i^*\right)$ of $\mathcal{L}$. The proof of Theorem 1 can be found in supplementary material.

4. Experiment

In this section, we evaluate the performance of the proposed method on two real-world multispectral images (MSIs).

4.1. Tensor completion task

To evaluate reconstruction performance, we employ three used metrics: Peak Signal-to-Noise Ratio (PSNR), Structural Similarity Index (SSIM), and Relative Squared Error (RSE). The proposed approach is compared with several representative tensor recovery methods, including high accuracy low-rank tensor completion (HaLRTC) [29], TNN [15], tensor completion by tensor factor-

Table 1
Evaluation metrics of MSI recovery results under different SRs.

Data	Method	SR = 5%			SR = 10%			SR = 15%			SR = 20%		
		PSNR	SSIM	RSE	PSNR	SSIM	RSE	PSNR	SSIM	RSE	PSNR	SSIM	RSE
Toy	Observed	11.169	0.251	0.975	11.407	0.287	0.948	11.659	0.323	0.921	11.923	0.357	0.893
	HaLRTC [29]	14.357	0.600	0.680	25.380	0.810	0.192	28.394	0.880	0.135	30.484	0.917	0.106
	TNN [15]	27.381	0.816	0.160	31.477	0.899	0.100	34.283	0.937	0.074	36.477	0.956	0.059
	TCTF [17]	27.453	0.764	0.156	31.965	0.866	0.096	34.464	0.913	0.075	36.505	0.937	0.060
	FTNN [22]	29.773	0.895	0.117	34.485	0.953	0.070	38.008	0.974	0.049	40.819	0.983	0.038
	UTNN [21]	28.912	0.860	0.128	35.066	0.950	0.062	38.925	0.976	0.040	41.855	0.986	0.029
	DTNN [24]	30.336	0.898	0.118	35.381	0.956	0.067	39.325	0.974	0.043	42.715	0.983	0.033
	Ours	**33.478**	**0.916**	**0.074**	**39.042**	**0.974**	**0.039**	**43.160**	**0.988**	**0.025**	**46.248**	**0.994**	**0.018**
Feathers	Observed	13.355	0.182	0.975	13.588	0.221	0.949	13.833	0.259	0.923	14.096	0.295	0.895
	HaLRTC [29]	16.726	0.590	0.660	24.660	0.795	0.265	27.467	0.864	0.192	29.772	0.907	0.148
	TNN [15]	26.445	0.737	0.221	31.982	0.880	0.120	34.604	0.925	0.091	36.787	0.950	0.072
	TCTF [17]	27.469	0.680	0.204	29.731	0.761	0.159	31.596	0.817	0.130	33.302	0.889	0.104
	FTNN [22]	29.480	0.881	0.157	33.928	0.947	0.097	37.248	0.969	0.069	39.903	0.981	0.053
	UTNN [21]	28.233	0.817	0.179	33.333	0.921	0.102	36.828	0.958	0.071	39.744	0.975	0.053
	DTNN [24]	29.023	0.830	0.183	33.322	0.920	0.114	36.954	0.958	0.080	39.888	0.973	0.063
	Ours	**31.542**	**0.881**	**0.128**	**37.317**	**0.960**	**0.068**	**41.338**	**0.982**	**0.045**	**44.667**	**0.990**	**0.033**

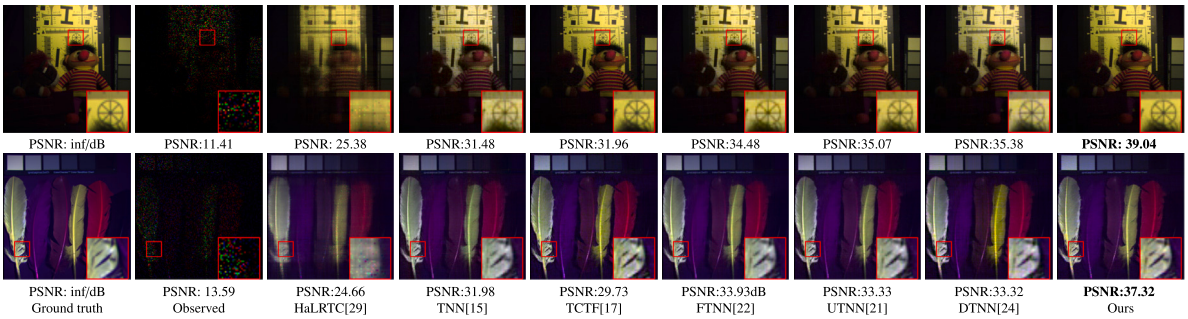

Fig. 1. Pseudo-color restoration results on MSIs (*Toy* and *Feathers*) at SR = 10% using different methods.

ization (TCTF) [17], framelet-based TNN (FTNN) [22], unitary-based TNN (UTNN) [21], and dictionary-based TNN(DTNN) [24]. Experiments are conducted under sampling rates (SRs) of 5%, 10%, 15%, and 20%. The numerical outcomes, summarized in Table 1, demonstrate that our model consistently yields the highest PSNR and SSIM scores together with the lowest RSE, indicating clear advantages in reconstruction accuracy. Representative visual comparisons at SR = 10% are presented in Fig. 1. In contrast to competing methods, our method preserves finer structures and suppresses artifacts more effectively, particularly in regions with intricate details. Overall, both quantitative measurements and visual inspections corroborate the superiority of the proposed framework over existing baselines.

4.2. Tensor compression task

For the compression experiments, we measure performance using the compression ratio (CR), defined as

$$\mathrm{CR} = \frac{\text{Number of factor elements}}{\text{Number of original tensor elements}} \times 100\%.$$

We also report the relative error (RE), given by $\mathrm{RE} = \|\mathcal{X}^* - \widehat{\mathcal{X}}\|_F^2 / \|\mathcal{X}^*\|_F^2$, where $\widehat{\mathcal{X}}$ represents the reconstructed tensor and $\mathcal{X}^*$ the ground truth. As baselines, we consider several widely used low-rank compression methods, including Tucker decomposition [30], TSVD(FFT) [31], and TSVD(DCT) [31]. Table 2 reports the CR and RE under various error tolerances on the two MSIs. Across all settings, the proposed method consistently achieves the lowest or competitive RSE while yielding the highest CR, especially under strict error constraints (e.g., RE = 0.004). Notably, for both datasets, the proposed method significantly outperforms HOSVD and TSVD-based methods in terms of compression efficiency without sacrificing reconstruction accuracy. These results highlight the superior representation capability of our method in high-fidelity tensor compression tasks.

5. Conclusion

In this paper, we introduced an it-product, which extends the classical t-product by allowing interactions between tensors with inconsistent third-mode dimensions through the introduction of alignment transform matrices. Based on the proposed it-product, we

Table 2
CR and RE for two MSIs under different error tolerances.

Data	Toy								Feathers							
Momel	RE = 0.01		RE = 0.008		RE = 0.006		RE = 0.004		RE = 0.01		RE = 0.008		RE = 0.006		RE = 0.004	
	CR	RSE	CR	RSE	CR	RSE	CR	RSE	CR	RSE	CR	RSE	CR	RSE	CR	RSE
HOSVD [30]	15.280%	0.010	19.440%	0.008	21.220%	0.006	33.020%	0.004	28.860%	0.010	35.880%	0.008	38.640%	0.006	67.490%	0.004
TSVD(FFT) [31]	29.763%	0.010	35.030%	0.008	42.540%	0.006	52.571%	0.004	37.223%	0.010	43.750%	0.008	52.344%	0.006	64.491%	0.004
TSVD(DCT) [31]	18.599%	0.010	22.051%	0.008	27.193%	0.006	34.778%	0.004	25.882%	0.010	29.738%	0.008	35.660%	0.006	45.010%	0.004
Ours	**10.358%**	0.010	**12.129%**	0.008	**15.918%**	0.006	**21.476%**	0.004	**17.812%**	0.010	**21.047%**	0.008	**25.272%**	0.006	**32.868%**	0.004

developed an efficient low-rank tensor factorization model for tensor completion and data compression tasks. To solve the resulting optimization problem, we designed a PAM-based algorithm and provided theoretical convergence guarantees. Extensive experiments on real-world multispectral images demonstrated that the proposed method consistently outperforms existing state-of-the-art tensor decomposition approaches, achieving superior reconstruction accuracy and compression efficiency. While the proposed model is for third-order data as presented, it is interesting to extend it to higher-order data for future work, such as light field images and color videos.

Appendix A. Supplementary data

Supplementary material related to this article can be found online at https://doi.org/10.1016/j.aml.2025.109770.

Data availability

Data will be made available on request.

References

[1] P. Wu, K.I. Kou, J. Miao, Efficient low-rank quaternion matrix completion under the learnable transforms for color image recovery, Appl. Math. Lett. 148 (2024) 108880.
[2] M.-M. Zheng, G. Ni, Approximation strategy based on the T-product for third-order quaternion tensors with application to color video compression, Appl. Math. Lett. 140 (2023) 108587.
[3] L.-B. Cui, W.-L. Hu, J.-Y. Yuan, Iterative refinement method by higher-order singular value decomposition for solving multi-linear systems, Appl. Math. Lett. 146 (2023) 108819.
[4] M. Ding, J. Yang, J.-J. Mei, Noisy tensor recovery via nonconvex optimization with theoretical recoverability, Appl. Math. Lett. 157 (2024) 109170.
[5] X. Mao, Y. Yang, T-product based ℓ_1-norm tensor principal component analysis and a finite-step convergence algorithm, Appl. Math. Lett. 160 (2025) 109318.
[6] F.L. Hitchcock, The expression of a tensor or a polyadic as a sum of products, J. Math. Phys. 6 (1–4) (1927) 164–189.
[7] L.R. Tucker, Some mathematical notes on three-mode factor analysis, Psychometrika 31 (3) (1966) 279–311.
[8] T.G. Kolda, B.W. Bader, Tensor decompositions and applications, SIAM Rev. 51 (3) (2009) 455–500.
[9] I.V. Oseledets, Tensor-train decomposition, SIAM J. Sci. Comput. 33 (5) (2011) 2295–2317.
[10] Q. Zhao, G. Zhou, S. Xie, L. Zhang, A. Cichocki, Tensor ring decomposition, 2016, arXiv preprint arXiv:1606.05535.
[11] Y.-B. Zheng, T.-Z. Huang, X.-L. Zhao, Q. Zhao, T.-X. Jiang, Fully-connected tensor network decomposition and its application to higher-order tensor completion, in: Proceedings of the AAAI Conference on Artificial Intelligence, Vol. 35, 2021, pp. 11071–11078.
[12] M.E. Kilmer, C.D. Martin, Factorization strategies for third-order tensors, Linear Algebra Appl. 435 (3) (2011) 641–658.
[13] E. Kernfeld, M. Kilmer, S. Aeron, Tensor–tensor products with invertible linear transforms, Linear Algebra Appl. 485 (2015) 545–570.
[14] S. Liu, X.-L. Zhao, J. Leng, B.-Z. Li, J.-H. Yang, X. Chen, Revisiting high-order tensor singular value decomposition from basic element perspective, IEEE Trans. Signal Process. 72 (2024) 4589–4603.
[15] Z. Zhang, G. Ely, S. Aeron, N. Hao, M. Kilmer, Novel methods for multilinear data completion and de-noising based on tensor-SVD, in: Proceedings of the IEEE Conference on Computer Vision and Pattern Recognition, 2014, pp. 3842–3849.
[16] C. Lu, J. Feng, Y. Chen, W. Liu, Z. Lin, S. Yan, Tensor robust principal component analysis with a new tensor nuclear norm, IEEE Trans. Pattern Anal. Mach. Intell. 42 (4) (2019) 925–938.
[17] P. Zhou, C. Lu, Z. Lin, C. Zhang, Tensor factorization for low-rank tensor completion, IEEE Trans. Image Process. 27 (3) (2017) 1152–1163.
[18] F. Wu, Y. Li, C. Li, Y. Wu, A fast tensor completion method based on tensor QR decomposition and tensor nuclear norm minimization, IEEE Trans. Comput. Imaging 7 (2021) 1267–1277.
[19] M. Zhou, Y. Liu, Z. Long, L. Chen, C. Zhu, Tensor rank learning in CP decomposition via convolutional neural network, Signal Process., Image Commun. 73 (2019) 12–21.
[20] C. Lu, X. Peng, Y. Wei, Low-rank tensor completion with a new tensor nuclear norm induced by invertible linear transforms, in: Proceedings of the IEEE Conference on Computer Vision and Pattern Recognition, 2019, pp. 5996–6004.
[21] G. Song, M.K. Ng, X. Zhang, Robust tensor completion using transformed tensor singular value decomposition, Numer. Linear Algebra Appl. 27 (3) (2020) e2299.
[22] T.-X. Jiang, M.K. Ng, X.-L. Zhao, T.-Z. Huang, Framelet representation of tensor nuclear norm for third-order tensor completion, IEEE Trans. Image Process. 29 (2020) 7233–7244.
[23] H. Kong, C. Lu, Z. Lin, Tensor Q-rank: new data dependent definition of tensor rank, Mach. Learn. 110 (7) (2021) 1867–1900.
[24] T.-X. Jiang, X.-L. Zhao, H. Zhang, M.K. Ng, Dictionary learning with low-rank coding coefficients for tensor completion, IEEE Trans. Neural Netw. Learn. Syst. 34 (2) (2023) 932–946.
[25] B.-Z. Li, X.-L. Zhao, T.-Y. Ji, X.-J. Zhang, T.-Z. Huang, Nonlinear transform induced tensor nuclear norm for tensor completion, J. Sci. Comput. 92 (3) (2022) 83.
[26] Y.-S. Luo, X.-L. Zhao, T.-X. Jiang, Y. Chang, M.K. Ng, C. Li, Self-supervised nonlinear transform-based tensor nuclear norm for multi-dimensional image recovery, IEEE Trans. Image Process. 31 (2022) 3793–3808.

[27] J.-L. Wang, T.-Z. Huang, X.-L. Zhao, Y.-S. Luo, T.-X. Jiang, CoNoT: Coupled nonlinear transform-based low-rank tensor representation for multidimensional image completion, IEEE Trans. Neural Netw. Learn. Syst. 35 (7) (2024) 8969–8983.
[28] M. Yang, L. Zhang, J. Yang, D. Zhang, Metaface learning for sparse representation based face recognition, in: 2010 IEEE International Conference on Image Processing, IEEE, 2010, pp. 1601–1604.
[29] J. Liu, P. Musialski, P. Wonka, J. Ye, Tensor completion for estimating missing values in visual data, IEEE Trans. Pattern Anal. Mach. Intell. 35 (1) (2012) 208–220.
[30] N. Vannieuwenhoven, R. Vandebril, K. Meerbergen, A new truncation strategy for the higher-order singular value decomposition, SIAM J. Sci. Comput. 34 (2) (2012) A1027–A1052.
[31] M.E. Kilmer, L. Horesh, H. Avron, E. Newman, Tensor-tensor algebra for optimal representation and compression of multiway data, Proc. Natl. Acad. Sci. 118 (28) (2021) e2015851118.